Project C3PO: In-Situ Tile Manufacturing for Lunar Landing and Launch Pads

Lance Ayers, Juan Barreto Jerez, Akash Bhukhanwala, Jonathan Celio, Ethan Cole, John Felt, Celine Gorkowski, Jonas Hoffmann, Maddy Layman, Vishnu Lella, Devon Rice, Sarvesh Srivastav *, and Dr. Kevin Shinpaugh†
Virginia Polytechnic Institute and State University, Blacksburg, VA, 24060

Project C3PO is a system designed to manufacture tiles from lunar regolith to develop launch and landing pads to support infrastructure development for a permanent lunar outpost. C3PO is a technology demonstration to test the manufacturing and performance of a small-scale landing pad. C3PO consists of two primary subsystems: SABER is a rover for site preparation, regolith excavation, tile placement, and site inspection, and KYBER is the tile manufacturing unit that sifts regolith, compacts regolith into a tile mold, and sinters the regolith via a thermal oven. The tiles features a symmetric, interlocking design, requiring only one tile mold to manufacture a landing pad. Tests with experimental samples sintered with LSP-2 simulant resulted in high compressive strength and temperature resistance. Although C3PO is a small-scale technology demonstration, all systems and the tile can be easily scaled to support large infrastructure development projects.

I. Introduction

In 2017, the United States government issued Space Policy Directive-1, outlining a return to the Moon. As humanity progresses in extraterrestrial operations, establishing permanent lunar infrastructure has become an essential objective for both governmental and commercial space agencies. The National Aeronautics and Space Administration's (NASA) Artemis Program and its commercial partners are taking steps to develop a long-term lunar base capable of supporting scientific, logistical, and industrial operations. The ability to construct durable, large-scale infrastructure using in-situ resources rather than relying exclusively on materials transported from Earth is imperative, as a primary challenge associated with lunar construction is the high cost and limited capacity of Earth-to-Moon transport [1].

The lunar environment also presents significant engineering challenges for complex systems. Systems deployed on the Moon must withstand highly abrasive lunar dust, extreme temperature fluctuations, a near-vacuum environment, micrometeorite impacts, and extended periods of darkness during lunar night [2].

To overcome these challenges in the face of vast potential, recent research aims to demonstrate the feasibility of manufacturing construction materials using in-situ resource utilization (ISRU) techniques within the lunar environment. With future missions such as Artemis, Starship, and Blue Origin landing on the Moon, building launch and landing pads is necessary to reduce the dust plumes generated by the exhaust of the lander. These pads serve as a lunar parking lot, where future landers can safely descend and be reused for repeated takeoffs and landings. This approach mitigates the effects of dust plumes containing regolith reaching speeds of 2000 $\frac{m}{s}$ or 4400 $\frac{mi}{hr}$ when a vehicle ascends or lands [3].

Lunar regolith is sharp and abrasive; therefore, nearby sensors and infrastructure can be damaged when the regolith moves at these high speeds [3–6]. The first point of contact for a spacecraft is the lunar surface. Therefore, constructing a landing pad that can reduce the effects of dust plumes during ascent or landing.

Team Cosmic Capstone Challenge Pad Operations (C3PO) is proposing the creation of novel, interlocking, ISRU tiles for the creation of launch and landing pads, or lunar parking pads. The proposed tile shall withstand the plume pressure and mechanical loads of future landers.

A. Mission and System Requirements

The system requirements shown in Table 1 were all derived from the RFP. System requirements 1.0, 2.0, 4.0, and 5.0 ensure that the payload is compatible with Griffin Lunar Lander (GLL). System requirements 3.0 and 7.0 ensure that the payload can withstand the lunar environment and lunar night. Lastly, system requirement 6.0 ensures that the payload can utilize resources on the lunar surface to develop infrastructure. These system requirements are expanded upon for each subsystem.

*Kevin T. Crofton Department Of Aerospace And Ocean Engineering Undergraduate Students
†Faculty Advisor and Collegiate Professor, Kevin T. Crofton Department Of Aerospace And Ocean Engineering

Table 1 Mission and System Requirements The requirements listed below apply to the entire system. All the system requirements were derived from the RFP.

ID	Description	Parent
SYS 1.0	The system shall have a mass less than 200kg.	RFP
SYS 2.0	The system shall have a volume less than 5.58 m^3.	RFP
SYS 3.0	The system shall survive the lunar night.	RFP
SYS 4.0	The system shall interface with the GLL.	RFP
SYS 5.0	The system shall communicate with the GLL..	RFP
SYS 6.0	The system shall demonstrate ISRU manufacturing capabilities.	
SYS 7.0	The system shall withstand lunar south pole environmental conditions.	RFP

B. Mission Architecture

Due to the 200 kg mass constraint, building a full-size landing pad is not feasible for the mission. Instead, the objective is to construct a technology demonstration using ISRU methods, such as sintering, and prove that the design can be scaled for larger missions.

To validate that the sintered tiles can withstand the forces of a lunar lander's takeoff and landing, numerical analysis is required. For this mission, the Griffin Lunar Lander's Attitude Control Thrusters (ACS) will be used. However, technical force data for the GLL is not available. To produce numbers for comparison, data from other landers, such as the Blue Origin Blue Moon lander, can be used to estimate. The Blue Moon lander has a landing mass of around 45,000 kg, an estimated exhaust temperature of $3400°C$, and an estimated plume pressure of 40 kPa. The leg force of the Blue Moon lander on the surface is 72.9 kN [7]. This data is a viable comparison because it is from a lander specifically developed to land on the Moon for near-future missions.

C3PO will employ two systems: Surface-Prep Analysis Building and Excavation Rover (SABER), and the Kiln for Yielding Building Elements from Regolith (KYBER). SABER is responsible for preparing the site by redistributing regolith to create a level surface for the lunar parking pad, placing tiles, and delivering regolith to KYBER. After delivery, the regolith is filtered out via an auger/hopper, placed into a tile mold, and sintered to form ISRU tiles. Once sintering is finished, the tiles require a cool-down period before placement.

SABER is responsible for site preparation, delivering regolith to KYBER, and placing the tiles. A robotic arm is used to excavate the pad area and place tiles. The chassis and suspension are made of aluminum and consist of a rocker-bogie suspension system. Following tile placement, the lunar parking pad will be inspected using LiDAR, thermal and optical cameras, a sun sensor, an Inertial Measurement Unit (IMU), and wheel encoders. In addition, mounted on SABER is a solar panel to help provide additional power for operations, and a Warm Electronic Box (WEB) is inside SABER to help keep the sensors insulated.

KYBER is a thermal oven that can produce sintered interlocking tiles that are made of 100% in-situ material. These novel tiles will be used to carry out C3PO's mission. KYBER is broken down into three main subsystems: regolith sifting and receiving, the tile mold, and the tile assembly method used to create structurally sound infrastructure. The system is about 35 kg and requires an average power of 355 W to ramp up and effectively sinter tiles. The lunar regolith is packed into a silicon carbide mold that is capable of withstanding repeat tile firings. KYBER is carried off of the GLL through SABER's robotic arm and placed onto the most accessible location of the lunar surface. Further discussion and imagery of the KYBER system can be seen in section II.B.

After system deployment, the small-scale lunar parking pad is tested under the firing conditions of the GLL ACS thruster. The lunar parking pad will have an area of $0.25m^2$, consisting of 16 diamond-up tiles and 9 diamond-down oriented tiles. The ACS thruster is manufactured by Agile Space Industries, which has a 2.4-inch diameter nozzle that produces 111.2 N of thrust when fired [8] under optimal conditions. To simulate the landing of a small class lander on the pad created by SABER, the ACS thruster is fired at the center of the pad. This test can determine whether the pad can survive future use.

C. Concept of Operations (ConOps)

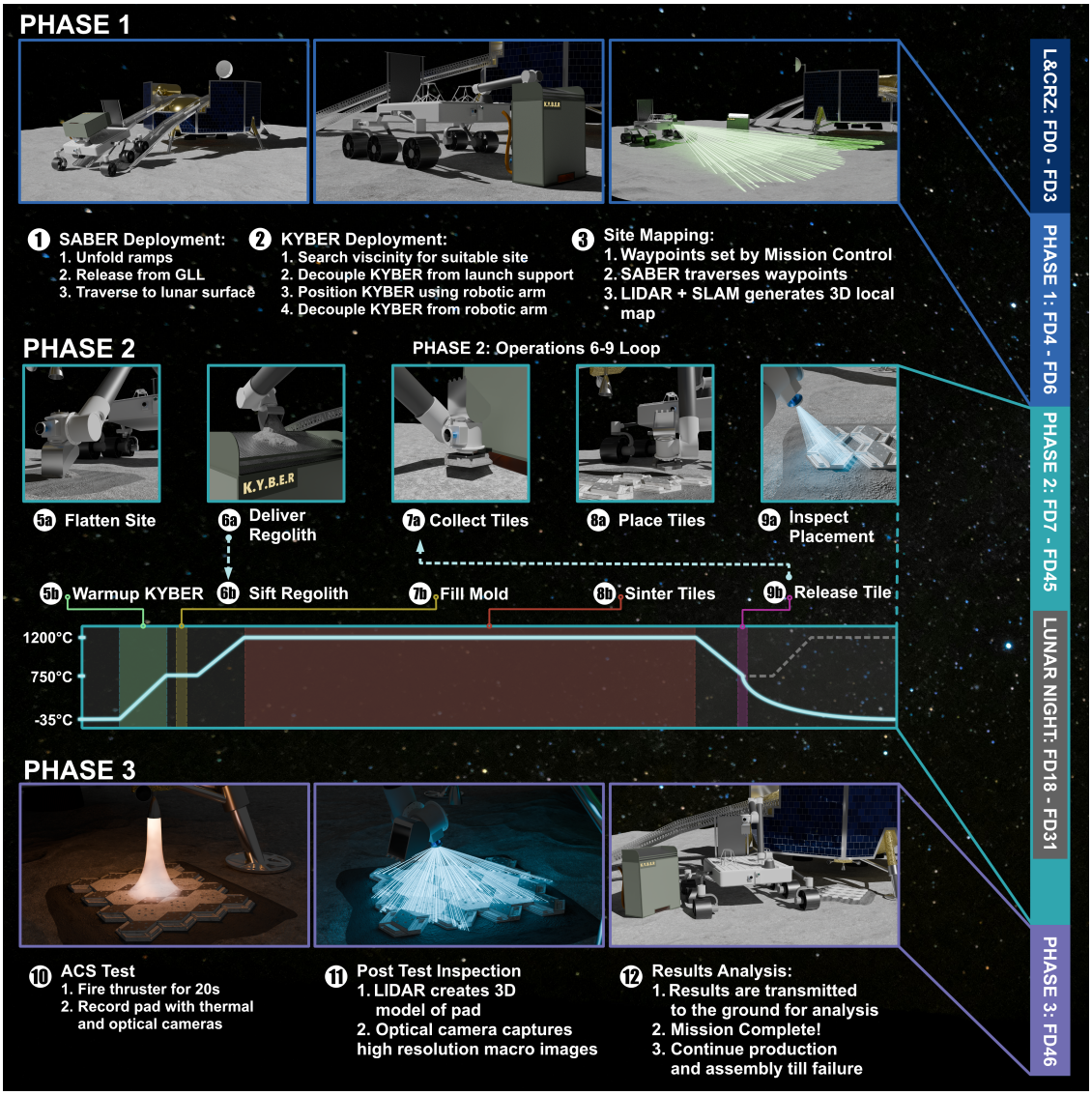

Fig. 1 3-Phase Concept of Operations. Phase 1 deploys and maps the site, Phase 2 autonomously fabricates and assembles regolith tiles, and Phase 3 performs pad testing and data collection.

The mission is structured into three sequential phases that progressively transition from deployment to production and validation. In Phase 1, the SABER rover and KYBER processing unit are deployed from the Griffin Lander (GLL) and conduct semi-autonomous site selection and high-resolution terrain mapping using LiDAR-based SLAM, establishing a suitable construction zone. Phase 2 constitutes the primary operational loop, in which regolith is excavated, processed, and sintered into tiles that are systematically placed to form a landing pad; this phase is fully autonomous and is interrupted by the lunar night cycle. During lunar night, operations are suspended and the system enters a survival mode to preserve thermal and power margins, resuming production once daylight conditions return. Thermal profiles are tightly controlled during sintering to ensure structural integrity, followed by inspection after placement. In Phase 3, the completed pad is subjected to a controlled plume impingement test using the lander's ACS thruster, while thermal and optical instrumentation capture performance data during and after testing. The results are transmitted to mission control for analysis, providing validation of in-situ resource utilization and construction techniques under representative lunar conditions.

II. System Summary and Constraints

A. Materials and Inspection

Materials and Inspection (MI) is tasked with creating interlocking tiles through the use of KYBER (Kiln for Yielding Building Elements of Regolith). These tiles will be used in the overall construction of future landing/launch pads for future lunar missions. The creation of theses tiles aim to mitigate the spread of dust plumes that are produced from thrusters of spacecraft that are trying to either take off or land.

1. Requirements

The MI subsystem requirements can be seen in Table 2. MI 1.0 states that the subsystem should minimize the production of lunar dust that is generated from thrusters. MI 2.0 aims to produce a tile that can withstand the thrust pressure force of the A110 thruster of 112 N [8]. MI 3.0 aims to produce a tile that can interlock and not easily be moved. MI 4.0 will produce a tile in under 24 hours using KYBER. MI 5.0 states that the produced tile will withstand the thermal load produced by the Griffin Lunar Lander. MI 6.0 shall produce enough tiles to form a test pad that is 0.25 m^2.

Table 2 MI Subsystem Requirements: MI 1.0 states the subsystem will minimize lunar dust plumes. MI 2.0 and MI 5.0 state that the produced tile will be able to withstand loads produced by the Griffin Lunar Lander. MI 3.0 sets the requirement that the tile must have an interlocking design. MI 4.0 sets the production time to be under 24 hours. MI 6.0 must produce enough tiles to create a 0.25 m^2 test pad.

ID	Description	Parent	Source
MI 1.0	The MI subsystem should minimize the generation of lunar dust.	SYS 7.0	
MI 2.0	The MI subsystem shall create a tile that can withstand 112 N of thrust.	SYS 6.0	Agile Space Industries [8]
MI 3.0	The MI subsystem should produce a tile that is interlocking.	SYS 6.0	
MI 4.0	The MI subsystem shall produce a tile in under 24 hours using KYBER	SYS 6.0	
MI 5.0	The MI subsystem shall create a tile that can withstand the thermal load of GLL.	SYS 6.0	
MI 6.0	The MI subsystem shall produce a test pad that is 0.25 m^2.	SYS 6.0	

B. KYBER

The materials and inspection team is responsible in the design and analysis of the system KYBER. KYBER is the thermal sintering system that will be used to carry out the overall mission that C3PO has to complete. KYBER is a thermal oven that can produce sintered interlocking tiles that are made of 100% in-situ material. KYBER is broken down into three main subsystems. The subsystems include sifting and receiving of the lunar regolith, the tile design and mold used to create the tiles that make up the lunar parking pad, and the tile assembly method used to successfully create structurally sound tiles. The entire system is about 35 kg and requires an average of 355 W of power to ramp up and effectively sinter the tiles. The lunar regolith is packed into a silicon carbide mold that is capable of withstanding the repeated firings that the mission requires. SABER will carry KYBER off of the Griffin Lunar Lander and onto the most accessible location on the lunar surface. SABER will deploy KYBER using the robotic arm it has attached as well as by exploding the pyro bolts that KYBER has attached. KYBER and its cross-section can be seen in Figure 2.

1. Material Receiving and Sifting

The lunar regolith grain size can vary between 40 and 800 μm [2]. However, to make the tiles, only grains smaller than 100 μm can be used [9]. Therefore, it is crucial to sift the material before it reaches the mold to remove oversized regolith and the occasional centimeter-sized rocks. The sifting mechanism used for this purpose consists of a vibrating triple-layer mesh placed at an incline on top of KYBER's receiving end [10, 11]. The mesh vibrations are generated by an electric vibrator like the ones used in material bulk handling on planet Earth. Each mesh layer has a different hole density to filter different regolith sizes. The top layer contains the lowest hole density to clear out the biggest grains first, and the middle layer is an intermediate step before reaching the bottom layer, which ensures that only grains under 100 μm reach the next processing stage. About 50 % of regolith on the Moon's surface is greater than 100 μm, ensuring a

(a) Internal View. **(b) KYBER External View.**

Fig. 2 KYBER Design. The images show the overall exterior design of KYBER as well as the internal cross-section. The overall components of KYBER and the subsystems the lunar regolith must go through can also be seen. These subsystems include sifting, collection, transportation, thermal sintering, and dispensing.

constant and consistent variation of regolith through the mesh [9]. The vibrating feature ensures the material keeps flowing and that unusable regolith is discarded to the side of KYBER, thanks to the inclined mesh configuration.

After being sifted, the regolith moves through a gradually narrowing hopper into a narrow passage leading to the compactor, which packs it into a mold. A rotating auger with variable speed improves material flow in the tightest sections. The mass and power per feed rate for the auger/hopper are estimated to be less than 10 $\frac{kg}{m^3hr}$ and 100 $\frac{W}{m^3hr}$, respectively [12].

2. Tile Design and Justification

To withstand the extreme environment on the lunar surface, there have been several proposed attempts that incorporate the tile approach. To compensate for abrasive regolith and integrate methods of ISRU, NASA has created a conceptual interlocking paver design. The design aims at demonstrating proper dust mitigation strategies as well as providing a baseline for reducing potential risks to equipment during operations [4, 13]. The European Space Agency (ESA) proposed this interlocking paver idea in a physical sense. By laser sintering directly onto simulated lunar regolith, the ESA produced hollow-centered triangular shapes in hopes of finding a way to create roads on the Moon [13]. C3PO aims in taking inspiration from both paver concepts while demonstrating IRSU capabilities to minimize the generation of lunar dust during operations.

The design for the paver concept, deemed a tile, C3PO has decided to implement a tessellation technique. This method implies producing tiles that fit together without any overlap while simultaneously tiling the plane. To increase the longevity and structural integrity of the tiles, the loads need to be evenly distributed [4, 14]. To achieve this, C3PO has created a tile, each of similar dimensions, that has both male and female connectors on one side shown in Figure 3.

The tile contains all protruding and recessing connectors on one face, enabling interlocking between adjacent tiles. The underside, diamond face down, of the tiles is a completely flat hexagonal shape that acts as a level base for a launch pad. Maintaining a uniform plane is essential for consistent, stable contact with the regolith. The holes on the top and bottom faces of the diamond are included to allow SABER to pick the tiles up and relocate them to the prepared construction site.

To evaluate tile performance, controlled test firings are conducted to collect thermal and mechanical data. Based on the provided thruster specifications, potential failures may happen within the design through thermal response and stress concentration. Under operating conditions, models developed in ANSYS establish the maximum thermal capacity of the tile through the distribution of heat flux from the heat plume generated by the 111.2 N from the thruster [8]. Through comparable heat flux values of light class landers, a heat flux of 3766.5 $\frac{kW}{m^2}$ is used for the thermal analysis.

With the thruster positioned 0.25 m vertically above the test surface, Figure 4 and Figure 5 display the heat flux distribution by means of temperature across the entirety of a single tile surface over a period of 20 seconds. This

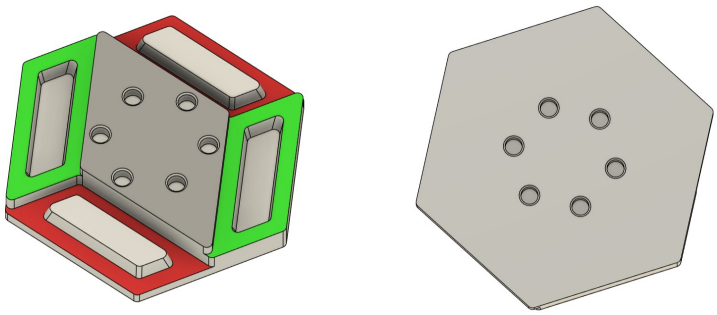

(a) Diamond-Up Tile Shape. **(b) Diamond-Down Tile Shape.**

Fig. 3 Image a shows male and female connectors for interlocking when set up in the diamond-up orientation. The portion of the tile with the red outline is where the connection is protruding, and the green outline indicates a recessed notch. Image b represents the diamond-down orientation on the flip side of the tile.

simulation duration illustrates the launch and landing associated with a lighter-class lander. In comparison, the Blue Moon from Firefly landing is estimated to be 20 seconds based on videos recorded from the landing [15]. For both the upward and downward facing diamond configurations, peak thermal loading is observed near the center of the tile where the heat flux in the plume is more focused, reaching a maximum temperature of 1609.1°C for the diamond down configuration and a maximum of 1617.6°C for the diamond-up configuration.

In contrast, lower temperatures of 1063.9°C were obtained on the top face of the diamond down configuration, excluding the vertices of the hexagonal shape. The diamond-up configuration experienced a higher minimum temperature of 1126.8°C.

Through thermal analysis, both tile orientations experienced elevated temperatures beneath the thruster nozzle, particularly in the holes used for placing the tiles. Considering the tiles are sintered at 1200°C for several hours, the varying composition of the lunar regolith indicates that the tile is capable of withstanding the imposed thermal loads from the thrusters without failure over the duration of the test. However, long-term fatigue on the tiles may occur due to localized heat flux based on the thermal gradient, which requires further investigation.

3. Tile Assembly

Tile assembly involves the permanent consolidation of loose lunar regolith into structural tiles for landing pad construction. Based on the trade study provided in the Appendix (Table **??**), traditional oven sintering was selected as the primary manufacturing method for the C3PO system. The oven configuration was chosen for its mechanical simplicity and superior system-level integration while meeting all requirements [16]. By utilizing 100% in-situ resource utilization (ISRU), sintering avoids the excess and compounding costs of transporting terrestrial additives, such as alkali binders, for geopolymerization, potentially saving hundreds of millions of dollars in launch costs over the mission lifetime [17].

Sintering functions by heating the regolith to a high (60-90%) percentage of its melting temperature, promoting diffusion between adjacent particles to form a cohesive solid without needing to reach a full liquid or molten state [16]. The primary advantage of operating at a lower temperature is the conservation of energy in sparse environments.

Within the KYBER subsystem, the tile assembly process is conducted through a dedicated oven assembly designed to produce 25 tiles composed entirely of lunar regolith. Each 1.2 kg tile is manufactured on a 10-hour cycle [16]. The thermal profile initiates at 750°C, ramps to a peak sintering temperature of 1200°C, and subsequently cools through ambient heat loss back to the baseline 750°C before the cycle repeats. To sustain these operations, the oven system utilizes 425 W per kilogram of regolith and maintains a total subsystem mass of 35 kg, remaining within the system mass and power budget. Figure 6 represents a simulation of the cooling for the tiles after 1 hour post-sintering.

This approach is more efficient in terms of power over full melting, as it avoids the higher heat requirements of a phase change while maintaining the stability and strength of the molded tiles during the cooling process. The selection is additionally supported by experimental results demonstrating that consistent sintering of lunar regolith simulant is achievable through radiant heating.

A significant factor in this selection is system complexity. Microwave systems require high-frequency components

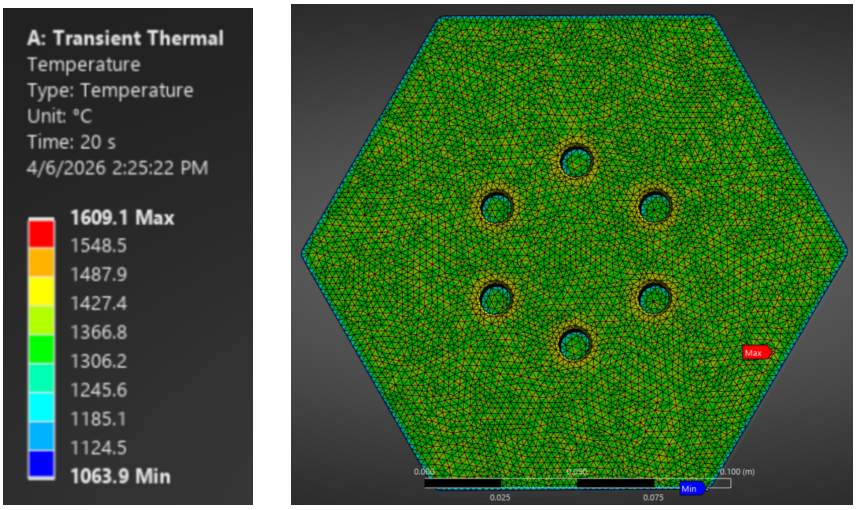

(a) Thermal Scale **(b)** Thermal Gradient over Tile-Diamond Down

Fig. 4 ANSYS Thermal Loading. Peak thermal loading on the diamond-down orientation of a singular tile due to a heat flux from the thruster plume. Image a displays the maximum and minimum temperatures achieved by the tile during the simulation. Image b displays the entire face of the diamond-down orientation, where the plume from the thruster is present during testing.

that pose substantial space-proofing challenges and introduce more failure points than traditional ovens. Furthermore, the oven architecture provides strong thermal consistency with the KYBER assembly. The insulation required for the oven is redundant with the thermal management necessary for the KYBER housing to prevent heat dissipation to the lunar environment or adjacent rover components. This integrated approach minimizes total system mass and ensures that thermal energy is efficiently contained within the sintering volume. Experimental validation, combined with the inherent simplicity of radiant heating, demonstrates that oven sintering is the optimal method for consolidating lunar regolith into structural tiles while satisfying all mission-critical requirements.

4. Tile Evaluation

A total of 50 images and five 20-second videos will be captured to evaluate pad performance under a controlled 20 s firing of the GLL ACS thruster at a distance of 0.25 m. Optical imaging from an arm-mounted camera records tile behavior during plume interaction, enabling post-test analysis of displacement, fragmentation, and ejecta velocity. This directly supports MI 1.0 by quantifying dust and particle generation, and MI 2.0 by assessing structural integrity under the applied 111.2 N thrust load.

Thermal performance is measured concurrently using a space-qualified infrared camera, such as the INO HDISCC, mounted on the main chassis to provide a stable, wide-field view of the pad. The system utilizes a 1024×768 VOx microbolometer array operating in the 3–14 μ band, with a noise-equivalent temperature difference of approximately 35 mK. These measurements enable precise characterization of tile heating and cooling transients, directly supporting MI 5.0 by evaluating thermal load resistance.

Testing is conducted on the interlocking tile pad with a total area of 0.25 m^2, satisfying MI 3.0 and MI 6.0, while prior fabrication constraints ensure compliance with MI 4.0 through sub-24 hour production using KYBER.

C. Preparation and Construction

Preparation and Construction (PC) is tasked with excavating the lunar surface to create a level surface for pad construction, delivering Lunar regolith to KYBER for creation of tiles, and placement of the sintered tiles acquired from KYBER. PC is also responsible for the inspection of the constructed Lunar Parking Pad to confirm the successful placement of the tiles and measure the pad's performance during testing.

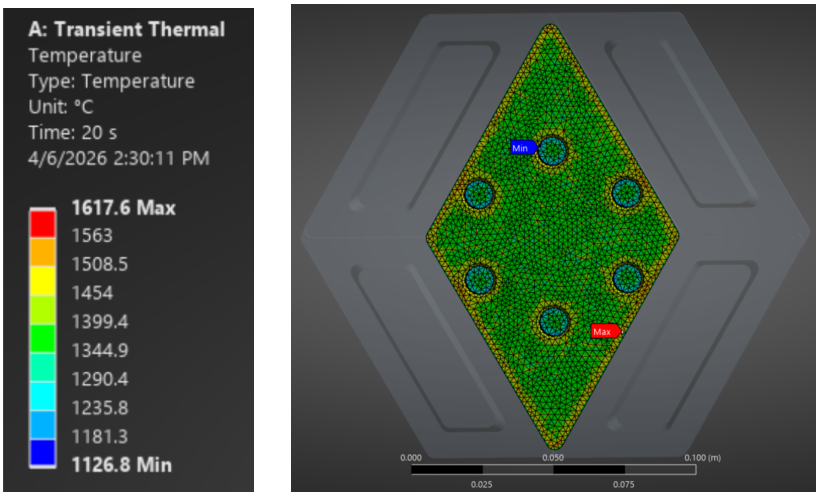

(a) Thermal Scale **(b)** Thermal Gradient over Tile-Diamond Up

Fig. 5 ANSYS Thermal Loading. Peak thermal loading on the diamond-up orientation of a singular tile due to a heat flux from the thruster plume. Image a displays the maximum and minimum temperatures achieved by the tile during the simulation. Image b displays the thermal gradient of the plume. Only the inner diamond portion displays a temperature profile as the remaining connectors are covered during the interlocking.

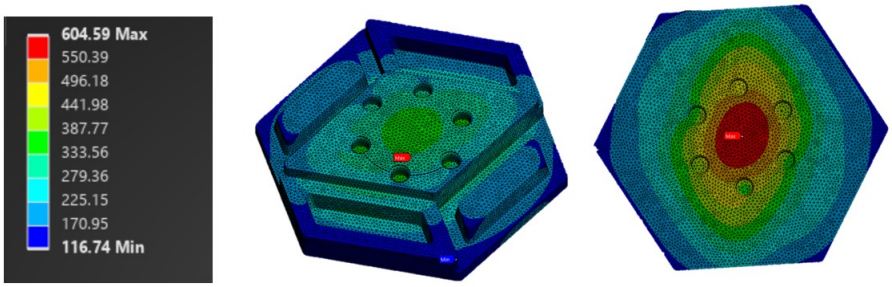

Fig. 6 ANSYS Ramp Down from 1200°C**.** Temperature of the tile after being sintered at 1200°C for 1 hour. The images show the highest and lowest temperatures after 1 hour of cooling for both tile orientations.

1. Requirements

The PC subsystems requirements can be seen in Table 3. PC 1.0 states the preparation size for the Lunar Parking Lot. The 1m x 1m preparation area is derived by the distance between adjacent legs on the Griffin Lunar Lander (GLL). The distance between legs is 2 meters the 1m x 1m preparation site allows room for maneuvering the SABER, the Surface-prep Analysis Building Excavation Rover. [18]. Preparing the surface to within two degrees of true level was derived from "Autonomous Multirobot Excavation for Lunar Applications" study where a pad of 3m x 3m was graded to within 0.4 meters of true level [19]. Scaling these results down, converting to an angle, then adding a 1.2x margin of error results in a 2° deviation across the pad. PC 2.0 will be fulfilled by having a sealed robotic arm and thermal regulations for all electronics. PC 3.0 is a value stated by MI. PC 4.0 depicts the necessity for PC to pickup the sintered tiles from KYBER. PC 5.0 and PC 6.0 are completed by a closed loop brushless dc motor and computer vision respectively. Lastly, PC 7.0 states the need to reduce the amount of moving parts used while manipulating Lunar regolith.

2. Excavation

Excavation is responsible for preparing a level site for the constructed launch pad. The selected method of excavation is a robotic arm with a scoop (RAS). Chosen due to an extended range of motion though degrees of freedom (DoF), a

Table 3 PC Subsystem Requirements PC 1.0 sets the boundaries for the Lunar Parking Pad. PC 2.0 and PC 7.0 state the environmental considerations. PC 3.0 gives the Lunar regolith delivery rate stated by MI. PC 4.0 depicts the need for collecting the sintered tiles from KYBER. Lastly, PC 5.0 and PC 6.0 states the placement and inspection accuracy given by MI and GNC.

ID	Description	Parent	Source
PC 1.0	The PC subsystem Shall prepare an area of 1 m by 1 m to within 2° of true level.	SYS 7.0	Astrobotics [18, 19]
PC 2.0	The PC subsystem Shall be tolerant to the Lunar environment.	SYS 3.0	
PC 3.0	The PC subsystem Shall supply KYBER with 0.1 kg/hour of Lunar resources.	SYS 7.0	MI
PC 4.0	The PC subsystem shall collect sintered tiles from KYBER	SYS 7.0	MI
PC 5.0	The PC subsystem Shall place ISRU units within 2 mm of target position.	SYS 7.0	MI, GNC
PC 6.0	The PC subsystem Shall confirm the placement of ISRU units to within 2 mm of target position.	SYS 7.0	GNC
PC 7.0	The PC subsystem Should minimize the generation of Lunar dust.	SYS 7.0	

trade study outlines the decision, which allows for precise material manipulation.

Using the RAS, a full scoop of lunar regolith is 7.81 kg. Incorporating the mass of the scoop, 8.07 kg, and 20 kg for the mass of the arm. A max total system mass of 35.88 kg was found. Powering the RAS with a Maxon EC 90 260 W brushless dc motor with a 100:1 gear ratio and constant 3 rpm motion. The gear box has an efficiency of 0.8 and the motor has an efficiency of 0.84 [20]. Combined the system has an efficiency of 0.67. Accounting for this loss of energy, a power of 3.67 Watts is consumed to operate the robotic arm per scoop of regolith.

To prepare the 1 m by 1 m to within 2° of true level to support the interlocking tiles, excavation begins within the immediate vicinity of SABER. At 3.67 Watts, the minimum number of full scoops required to clear the area is 53 scoops. The length from the base of the robotic arm to the scoop on the fifth DoF is 0.84 m fully extended. With this range, the RAS cannot clear the entire area underneath of the lander without repositioning, if there was no major major regolith displacement from the lander plume. As the RAS has 6 DoF total, the lander may obstruct the excavation process as well.

3. Material Delivery

Using the same RAS calculation as above, a max load power of 3.67 watts was found for material delivery. The max capacity of KYBER is 24 kg of regolith. A total of three scoops is needed to fill KYBER. SABER will deliver three full scoops to KYBER fulfilling PC 3.0 by delivering at least 0.1 $\frac{kg}{hr}$ of Lunar regolith. The mass of a single tile is 1.2 kg, therefore to create 25 tiles two full loads of regolith will be delivered. Assuming the rover always has to travel the max working distance of 20 m, GNC 3.0, and the rover is traveling at a constant speed of 0.1 $\frac{m}{s}$, stated my SM, a max total energy of 14.68 Wh is consumed. Mass and power specifications can be seen in Table 4

4. Tile Placement

The tile placement subsystem uses a lightweight articulated robotic arm, shown in Fig. 7, capable of operating in excavation, tile placement, and stowed configurations. As summarized in Table 5, the manipulator combines low mass, high placement precision, and low energy consumption, making it well suited for repeated autonomous construction operations on the lunar surface. Its end-effector accuracy and repeatability are sufficient for reliable alignment of adjacent tiles with minimal cumulative geometric error, while its modest deployment and operating power requirements help keep the overall pad construction process within the system's strict energy and thermal constraints. In particular, the low energy required for both KYBER deployment and tile placement indicates that the arm can execute repeated construction tasks without placing significant demand on the rover power budget.

Table 4 Material Delivery Mass and Power Budget. Scoop refers to the mass of just the scoop attachment. Full scoop of regolith gives the max mass of regolith the scoop is able to hold. Full scoop + scoop states the power and energy consumed by collecting one scoop of regolith, also giving the mass of the full scoop + scoop neglecting the mass of the arm. Material delivery depicts the power and energy consumed per scoop delivered to MI, now including the mass of the arm. Lastly, material delivery for the mission lifespan shows the power and energy consumed over all twelve actions throughout material delivery, alongside the max mass throughout the process.

Action	**Power (W)**	**Mass (kg)**	**Energy (Wh)**
Scoop	N/A	8.07	N/A
Full Scoop of Regolith	N/A	7.81	N/A
Full Scoop + Scoop	3.67	15.88	0.0068
Material Delivery	3.67	35.88	0.408
Material Delivery (Mission Lifespan)	3.67	35.88	2.45

Table 5 Robotic arm mass, positioning performance, and power requirements for tile placement operations.

Parameter	**Value**
Arm mass	20.92 kg
End-effector accuracy (RSS)	0.982 mm
End-effector accuracy (worst-case)	1.636 mm
End-effector repeatability (RSS)	0.106 mm
End-effector repeatability (worst-case)	0.177 mm
KYBER deployment mechanical power	40.8 W
KYBER deployment electrical power	60.715 W
KYBER deployment thermal power	19.914 W
KYBER deployment time	10.0 s
KYBER deployment energy	0.169 Wh
Tile placement electrical power	2.045 W
Tile placement thermal power	0.671 W
Tile placement energy	0.034 Wh
Total energy for pad construction	0.852 Wh

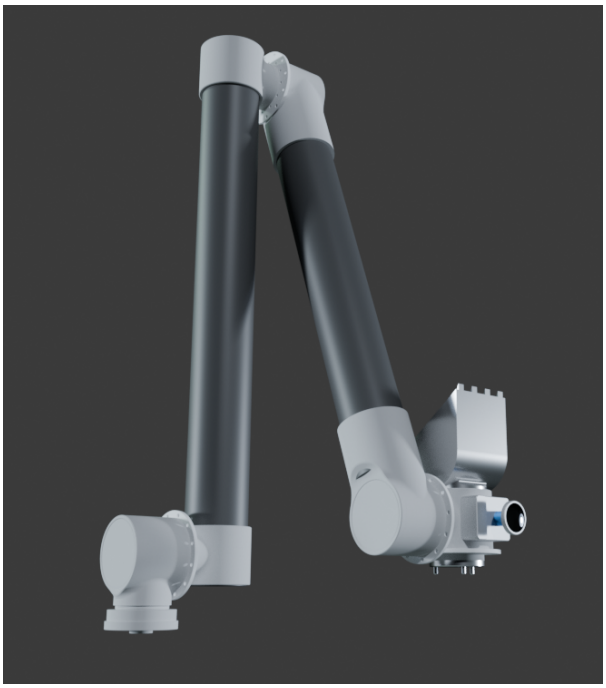

Fig. 7 6 DoF robotic arm used for tile placement, excavation, surface preparation, and material delivery on SABER. The robotic arm includes two tools, the first being a scoop for preparing the tile placement surface, excavating regolith, and delivering regolith to KYBER. The second tool is a custom-made end effector that features a 3-pronged gripper that can squeeze and release to grab and place tiles.

5. Site Inspection

Site inspection is responsible for verifying that the constructed landing pad meets geometric, placement, and thermal performance requirements defined in the Preparation and Construction (PC) requirements set. In particular, inspection directly supports compliance with PC 1.0 (surface flatness within 2°), PC 5.0 (tile placement within 2 mm), and PC 6.0 (verification of placement accuracy). During construction, surface geometry is characterized using a scanning LiDAR system mounted on the main chassis of SABER to generate a high-resolution topographic map of the prepared site. Space-qualified LiDAR systems such as the GSFL-16 provide millimeter-scale ranging precision, enabling verification

of flatness and planarity well within the < 1 mm measurement error margin [21]. This provides sufficient margin to ensure compliance with the 2° leveling requirement in PC 1.0 by enabling reconstruction of surface slope across the pad footprint. Additionally, LiDAR mapping enables detection of local deviations that could lead to uneven load distribution during landing.

Complementing LiDAR, a high-resolution optical camera (e.g., CASPEX 4M with IRIS optics) is mounted on the robotic arm to enable close-up inspection of tile placement. This configuration allows direct verification of Tile Placement Accuracy (TPA) at the individual tile level, ensuring compliance with PC 5.0 and PC 6.0. Vision-based methods can resolve features on the order of 1–5 mm depending on illumination conditions [22], providing sufficient accuracy to confirm placement within the 2 mm tolerance requirement. The robotic arm placement is critical, as it enables inspection from multiple viewing angles and distances, mitigating occlusions and improving measurement confidence. Together, the LiDAR and vision systems provide complementary global and local measurements required to certify pad geometry and tile placement prior to testing.

Table 6 Inspection hardware and performance characteristics. Prepared Surface Quality (PSQ) supports verification of PC 1.0 by quantifying global flatness, slope, and planarity. Tile Placement Accuracy (TPA) supports PC 5.0 and PC 6.0 by measuring tile alignment and interlocking within millimeter tolerances. Thermal Inspection (TI) supports PC 2.0 and PC 7.0 by measuring heat retention and plume-induced thermal effects, which correlate with material survivability and dust generation behavior.

Technique	**Measured Attributes**	**Mass (kg)**	**Power (W)**	**Error**	**Notes**
LiDAR	PSQ, TPA	3.2	30	< 1 mm	Chassis-mounted, large range, lighting independent
Vision	TPA	~ 0.5	1.5	< 1 mm – 5 mm	Arm-mounted for close inspection, lighting dependent accuracy
IR Camera	TI	~ 0.5	1.5	0.035 °C	Chassis-mounted, integrated with primary camera system

D. Structures and Mobility

The Structures and Mobility (SM) subsystem primarily concerns the SABER's chassis, suspension, and wheels. It is designed to ensure the structural integrity of the rover while traversing the lunar south pole terrain and withstanding operational loads.

1. Requirements

The mission-level SM requirements are shown in Table 7. The temperatures on the surface of the moon can vary between 40 and 400 K [23]. Therefore, SM 1.0 indicates that all structural components shall be able to operate under such conditions. SM 2.0 is derived from the RFP, which specifies that 3/4 of the GLL's total payload volume, 5.58 m^3, can be used for this mission. The traversing area in SM 3.0 was determined by accounting for the limitations of the CCDH and GNC subsystems. The median slope of the terrain on the lunar south pole is around 7.6°and can reach above 25°at some of the steepest sections [24]. Therefore, SM 4.0 was formulated to enable the rover to operate on the steepest terrain if needed. The 30 cm obstacle height was chosen because boulders with a diameter under 50 cm tend to be more abundant, and the cumulative fractional area of rocks increases as their diameter decreases [25–27]. So, a carefully chosen landing site and the ability to traverse obstacles up to 30 cm in height will allow the rover to overcome most obstacles.

2. Rocker-bogie suspension

The rocker-bogie suspension system, shown in Figure 8, was selected for its simplicity and proven legacy in interplanetary missions. Each side of the suspension consists of a freely rotating bogie attached to a rocker that pivots around a bar connected to a differential mechanism, as seen in Figure 8a. The differential mechanism allows each side of the suspension to rotate in the opposite direction to its counterpart, keeping all wheels on the ground at all times. The

Table 7 SM Requirements used for system evaluation. The system requirements were chosen to guarantee a successful mission from the structural and mobility standpoint. They address volume, structural, and traversability constraints.

ID	Description	Parent	Source
SM 1.0	The structural components of the vehicle shall withstand surface temperature fluctuations between 40 and 400 K.	SYS 3.0, 7.0	[23]
SM 2.0	The total volume of the vehicle shall fit in a 1.7 m x 1.75 m x 1.875 m space inside the GLL.	SYS 1.0, 4.0	RFP
SM 3.0	The vehicle shall be able to traverse inside a radius of 20 m from the lander.	SYS 6.0	GNC
SM 4.0	The vehicle shall be able to traverse slopes and obstacles up to 25° and 30 cm of height, respectively.	SYS 6.0, 7.0	[24, 25]

chassis always maintains the average pitch angle of both rockers [28]. In addition, this suspension allows the rover to climb obstacles up to twice the wheel diameter. However, due to the lack of springs and damping mechanisms, dynamic shocks must be prevented to preserve structural integrity, making this suspension better suited to low speeds. Therefore, the maximum speed was set to be 0.1 m/s.

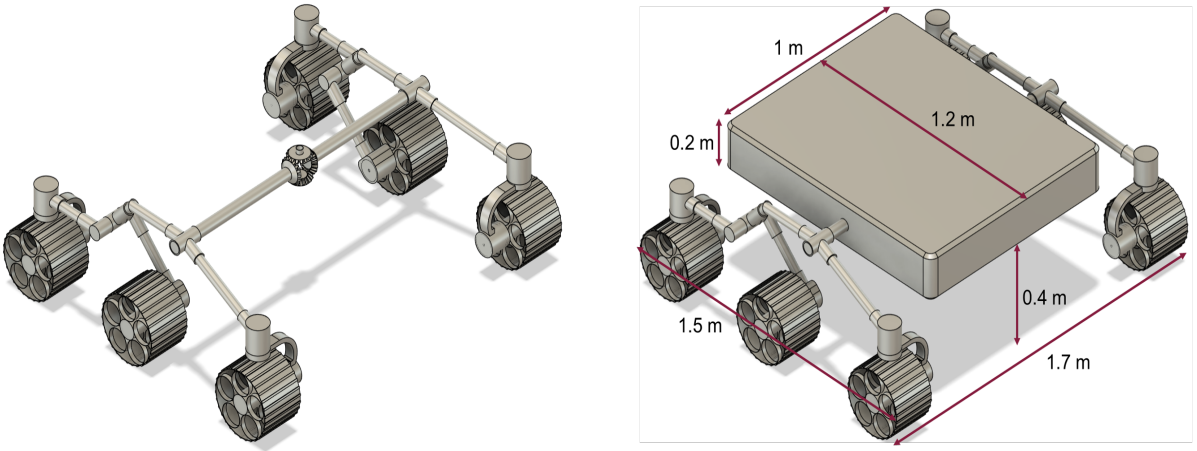

(a) Rocker-bogie suspension with differential gears. **(b)** Rocker bogie suspension and rover chassis with dimensions.

Fig. 8 a) The rocker-bogie suspension uses differential gears to rotate each side in the opposite direction of the other, helping the chassis maintain the average pitch angle of both rockers. b) The rover dimensions where designed to fit in a 5.58 m^3 space inside the GLL.

The aluminum bars making up the suspension have a diameter of 4 cm and a thickness of 0.2 cm. The suspension's structural integrity was evaluated using a simple finite element model with 1D bar elements under static conditions. Under this model, the suspension was able to withstand its own weight and point loads of 650 N at the rocker pivot point, which are significantly higher than the loads expected for this mission. The chassis is also made of aluminum, with dimensions of 1000x1200x200 cm and a wall thickness of 0.3 cm. The rover dimensions are shown in Figure 8b. The distance between the ground and the bottom of the chassis is 40 cm.

3. Wheels and motors

The motors that SABER utilizes to traverse across the lunar surface are the EC 90 flat Ø90 mm, brushless, 260 W, with Hall sensor motors [20]. SABER utilizes 10 of these motors along with 10 gearboxes, the SHF-20-160-2UH, to achieve the desired torque [29]. Six of these brushless motors drive SABER's wheels across the lunar surface, while the other four are used to steer the front and back wheels. The motors and gearboxes that SABER uses produce the 6 Nm of torque required to move SABER at a maximum speed of 0.1 m/s. To calculate the required torque that each of the wheels

would need to traverse the surface of the moon, equation 1, was implemented. It accounts for the rolling resistance force, the rover's weight, and the required force to reach a maximum acceleration of 0.02 $\frac{m}{s^2}$. m, g, μ, θ, and a correspond to the maximum allowed mass of 200 kg, lunar gravity, coefficient of rolling resistance of 0.3, maximum terrain inclination of 30°, and maximum acceleration, respectively. Conservative values were selected for these calculations to ensure the mobility system meets the mission requirements and to account for simplifications in the methodology.

$$\tau_{wheel} = \frac{1}{6} r(mg(\mu \cos\theta + \sin\theta) + ma) \tag{1}$$

The wheels utilized in SABER are flexible metal wheels. They are used for SABER due to their flexibility and strength, which allow them to increase the contact area with the terrain while withstanding operational loads. The structure of the wheel consists of a rigid inner cylindrical hub surrounded by 3 rows of spring loops. The rim of the wheel is a thin sheet surrounding the spring loops, giving the wheel a dampening effect on the rover. The rim and spokes are made up of spring steel to improve wheel elasticity, while the hub is made of aluminum to improve the wheel's sturdiness. The diameter and width of each wheel are 0.28 m and 0.2 m, respectively [30].

4. Mass, power, and cost estimates

The combined mass of the suspension, chassis, steering motors, and drive motors was determined to be 94.2 kg. The power required for the mobility system was estimated to be 35 W by using Equation 2, in which $P_{rolling}$ is the total electric power required to move the wheels. v represents the maximum rover velocity of 0.1 m/s. This estimate also assumes a motor efficiency of 70%. The expected cost of the suspension and chassis was estimated as 20 M USD.

$$P_{rolling} = 1.3vmg(\mu \cos\theta + \sin\theta) \tag{2}$$

E. Guidance, Navigation, and Control (GNC)

The Guidance, Navigation, and Control (GNC) subsystem enables the C3PO rover to autonomously and semi-autonomously traverse and operate within a constrained lunar workspace. The subsystem is responsible for estimating the rover state, constructing and maintaining a map of the environment, generating feasible trajectories, and executing control actions to achieve mission objectives. Because the lunar environment lacks Global Navigation Satellite System (GNSS) infrastructure and presents extreme lighting and terrain conditions, the GNC system must rely entirely on onboard sensing and computation. For this reason, the architecture is based on LiDAR-inertial Simultaneous Localization and Mapping (SLAM), a well-established technique for navigation in GPS-denied environments [31, 32]. Similar approaches have been successfully deployed in planetary exploration missions, where onboard autonomy is required due to communication latency and limited operator intervention [33].

1. Requirements

The mission-level GNC requirements define constraints on navigation accuracy, operational range, and environmental survivability, as summarized in Table 8. These requirements are derived from system-level mobility and payload constraints and directly inform the selection of sensing modalities, estimation algorithms, and control strategies.

Table 8 GNC Requirements used for system evaluation

ID	Description	Parent	Source
GNC 1.0	The GNC subsystem shall maneuver the rover within 0.1 m of a desired waypoint.	PC 5.0	
GNC 2.0	The GNC subsystem shall estimate rover pose with an accuracy of ≤ 0.1 m.	GNC 1.0, PC 5.0	[32]
GNC 3.0	The GNC subsystem shall maintain navigation performance within 10 m (2x GLL) radius of the landing site.		
GNC 4.0	GNC subsystem components shall operate within a survival temperature range of -40 °C to 85 °C.	SYS 3.0	[34]

The navigation accuracy requirements are driven by the need to execute precise waypoint-based tasks such as regolith collection and site preparation. Operational range was determined by the GLL's deployment radius, with a 2x margin for maneuvering. The survivability requirement enforces the use of space-qualified components, which must be protected from the extreme thermal conditions of the lunar surface.

2. GNC Architecture

The GNC system is organized into a hierarchical control structure consisting of full autonomy, semi-autonomy, and mission control, as illustrated in Figure 9. This architecture was selected to balance onboard decision-making capability with the need for supervisory oversight, ensuring both operational efficiency and fault tolerance.

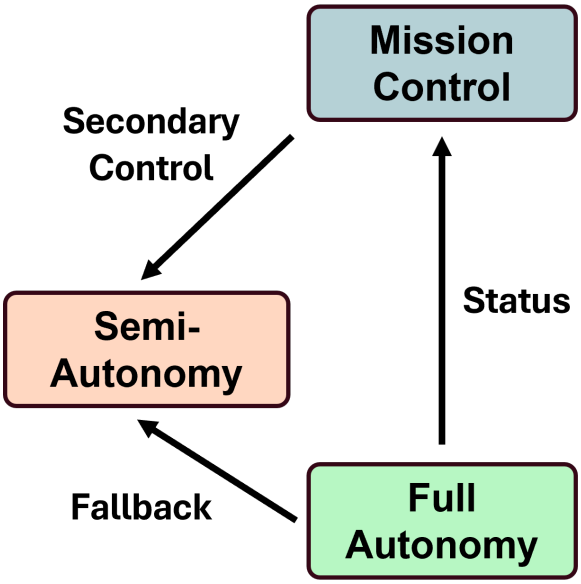

Fig. 9 GNC guidance architecture and control flow. The guidance system generates reference trajectories and control objectives based on mission goals, which are processed by control algorithms to produce actuator commands. This architecture ensures stable and responsive vehicle behavior during all operational phases.

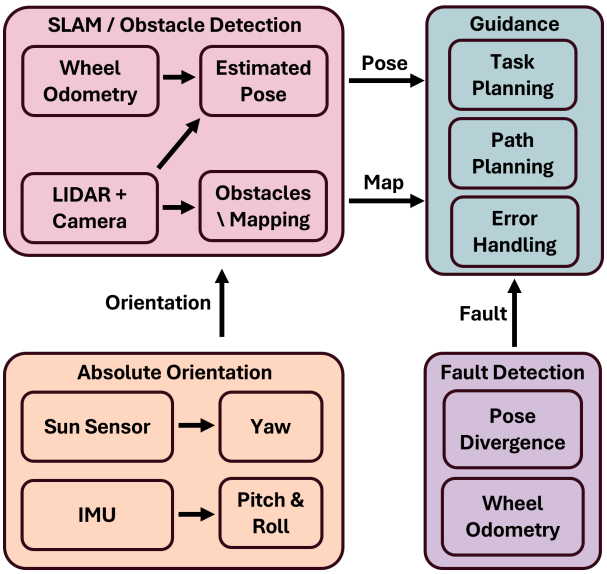

Fig. 10 Navigation architecture flowchart. The navigation system fuses sensor measurements to estimate vehicle state, providing accurate position, velocity, and attitude information to support guidance and control functions.

In full autonomy mode, the rover executes tasks independently using onboard perception and planning. This mode is the primary operating state following initialization, as it minimizes reliance on communication with the lander and allows continuous operation despite latency or intermittent connectivity. Semi-autonomous mode is used during initialization, fault recovery, or complex operations where higher-level input is beneficial. In this mode, mission control provides waypoint commands or task directives, while the rover retains responsibility for local navigation and obstacle avoidance. Mission control provides supervisory oversight, monitors system health, and can intervene if anomalous behavior is detected. The inclusion of multiple control modes ensures that the system can degrade gracefully in the presence of faults, with semi-autonomy acting as a fallback when confidence in autonomous operation is reduced.

3. Navigation Architecture and Sensor Fusion

The navigation architecture integrates multiple sensing modalities to provide robust and redundant state estimation, as shown in Figure 10. The system combines LiDAR, camera data, wheel odometry, inertial measurements, and a sun sensor to estimate both relative and absolute pose.

LiDAR serves as the primary sensing modality for mapping and obstacle detection due to its ability to generate high-resolution geometric measurements independent of ambient lighting conditions. Wheel odometry provides

short-term motion estimates with low computational cost but is subject to drift due to wheel slip, which is expected in loose regolith. The inertial measurement unit (IMU) provides high-frequency motion propagation and orientation estimates, while the sun sensor provides an absolute heading reference that helps bound long-term drift. [31].

The sensing suite that enables this fusion architecture consists of a GSFL-16 LiDAR unit, a Safran STIM377H IMU, wheel encoders, a nanoSSOC-D60 sun sensor, and auxiliary optical and thermal cameras. Collectively, these components define the dominant sources of uncertainty in the localization solution and provide the physical basis for the error model developed in the following sections.

4. Simultaneous Localization and Mapping (SLAM)

Simultaneous Localization and Mapping (SLAM) is the core algorithmic framework used by the GNC subsystem. SLAM enables the rover to estimate its position while concurrently building a map of an unknown environment. This is achieved by combining motion predictions with sensor observations and optimizing the resulting state estimates to minimize accumulated error [32].

In this implementation, SLAM operates in a closed-loop manner. The rover first propagates its pose using inertial and odometry measurements, a process commonly referred to as dead reckoning. These estimates are then corrected using LiDAR scan matching, in which new scans are aligned with previously observed data or a constructed map. As the rover revisits previously mapped areas, loop closure constraints are introduced, allowing the system to correct accumulated drift through global optimization. This process significantly improves long-term accuracy and is essential for reliable navigation over extended traverses.

5. Mission Navigation Flow

The GNC system follows a two-phase operational strategy that reflects the differing requirements of initial exploration and sustained mission operations. Upon deployment, the rover enters an initial mapping phase in which it performs exploratory motion to construct a representation of the workspace. During this phase, the system relies primarily on dead reckoning and local SLAM without enforcing loop closure. This approach reduces computational complexity and allows rapid map generation, albeit with increasing drift over time.

Once sufficient coverage of the workspace has been achieved, the system transitions to a closed-loop SLAM mode. In this operational phase, loop closure detection is enabled, and the map is globally optimized to reduce accumulated error. The improved localization accuracy allows the rover to execute waypoint-based tasks with high precision. This phased approach is widely used in robotic exploration, as it balances the need for rapid initial mapping with the requirement for accurate long-term navigation [32].

6. GNC Components

The GNC subsystem utilizes a set of sensors selected to provide complementary capabilities while satisfying mass, power, and environmental constraints. The Safran STIM377H IMU provides high-precision inertial measurements with low bias instability, making it suitable for navigation in GNSS-denied environments [35]. The GSFL-16 LiDAR serves as the primary perception sensor, enabling accurate mapping and obstacle detection [21]. The CASPEX 4M camera and associated optics provide visual context and support perception tasks [22], while the INO HDISCC thermal camera enables operation in low-visibility or extreme lighting conditions [36]. The nanoSSOC-D60 sun sensor provides an absolute orientation reference, which is particularly valuable for correcting long-term heading drift [37]. Wheel encoders provide direct measurements of wheel rotation, enabling short-term motion estimation [38].

A summary of the GNC subsystem mass, power, and cost is provided in Table 9. These values represent estimated contributions from each sensor component and are used to verify that the subsystem remains within overall mission constraints.

7. GNC Subsystem Design Summary

The final GNC subsystem integrates LiDAR-inertial SLAM, multi-sensor fusion, and a hierarchical autonomy structure to enable reliable navigation in a constrained lunar environment. The use of SLAM allows the rover to operate without external positioning infrastructure, while loop closure ensures long-term accuracy. The combination of complementary sensors mitigates individual failure modes, and the control architecture enables graceful degradation in

Table 9 GNC System Resource Budget

Component	Mass (kg)	Power (W)	Cost ($)
GSFL-16 LiDAR	3.2	30	~100,000
CASPEX 4M Camera + IRIS 25mm	0.062 + ~0.5	1.5	~40,000
INO HDISCC Thermal Camera + Lens	0.5 + 0.25	1.7	~60,000
nanoSSOC-D60 Sun Sensor	0.0065	0.01	4,400
STIM377H IMU	0.055	1.5	10,000
VLS-25-II Wheel Encoders (6)	0.036	2.7	~7,200
Total	**~4.65**	**38**	**~230,000**

the presence of faults. This design provides a robust and efficient solution for autonomous lunar surface operations, consistent with established practices in planetary robotics.

F. Command, Communications, and Data Handling

The communications, commands, and data handling (CCDH) system is responsible for developing and maintaining the communication architecture and data management framework that enables C3PO's lunar system to operate reliably and intelligently.

1. Requirements

The mission-level CCDH requirements that govern subsystem design and evaluation are summarized in Table 10. CCDH 1.0 defines transmission of payload health metrics to the lander such as system heartbeat, battery health, and temperature. CCDH 2.0 establishes the requirements for a safe state fallback during instances of connection loss. CCDH 3.0, 5.0, and 6.0 cover the necessary network protocols and modem compatibility standards. CCDH 4.0 refers to the wireless connectivity range between the lander and the payload. A radius of 150m–200m is the standard range for a Wi-Fi module. CCDH 7.0 is derived from the GNC camera selection and the MI and PC photo and video necessities. As specified by the MI, PC, and GNC subsystems, the C3PO system must be able to send 50 images and 5 20-second videos to the GLL to downlink to ground. Each photo taken by the CASPEX 4M camera has roughly a 4 megapixel resolution, which equates to $\sim$ 12.5 bytes. The CASPEX 4m records videos in 16 frames/second, making a 20-second video about 168 bytes. For 50 pictures and 5 20-second videos, the total minimum amount of data required to transfer back to ground is $\sim$ 1.5 GB.

2. Wired Communication

The Astrobiotic GLL user guide recommends that payloads have the ability for both wired and wireless connections. The GLL has the capability for an RS-422 or SpaceWire wired connection. RS-422 supports point-to-multidirectional two-way communication over twisted-pair cables, has a maximum transmission distance of about 1219 meters, and a maximum transmission rate of 10 Mb/s [41]. SpaceWire provides high-speed, bi-directional, full-duplex, data links and is designed to connect electronic components such as high data-rate sensors, processing units, and memory devices onboard spacecraft. [42].

3. Wireless Communication

Since the payload will be detached from the lander, wireless communication with the GLL is required. According to Astrobotic guidelines, the Wi-Fi module should be able to connect using 2.4 GHz Wi-Fi with the 802.11n WLAN standard. The 802.11n protocol employs a multiple-input multiple-output (MIMO) scheme, which contributes to increased data transfer speed and utilizes multiple antennas for enhanced signal reliability. Since the rover will operate only a few meters from the lander, the Wi-Fi module should not deviate too far from the acceptable range. Due to this small test envelope an external antenna is not needed. Space-rated Wi-Fi modules have operating temperatures of -40 °C to 85 °C; however, lunar temperature ranges from -157 °C to 120 °C, therefore, additional thermal techniques are

Table 10 CCDH Requirements used for system evaluation. The table lists the six mission-level CCDH requirements relevant to the payload's data management and communication architecture. Requirements CCDH 5.0 and 6.0 are derived directly from the GLL.

ID	Description	Parent	Source
CCDH 1.0	The CCDH subsystem shall send data to the lander on payload health	SYS 4.0	
CCDH 2.0	The CCDH subsystem shall establish a safe state fallback for when wireless connection to lander drops	SYS 4.0	
CCDH 3.0	The CCDH subsystem shall establish IP protocols	SYS 4.0	
CCDH 4.0	The CCDH subsystem shall ensure wireless connectivity between the lander and the payload up to 150 m radius from the lander	SYS 4.0	[39, 40]
CCDH 5.0	The CCDH subsystem must insure that the payload is 802.11n WLAN modem compatible	SYS 1.0, 4.0, 6.0	[18]
CCDH 6.0	The CCDH subsystem must insure that the payload follows RS-422 / SpaceWire protocols	SYS 4.0	[18]
CCDH 7.0	The CCDH subsystem shall be capable of handling 1.5 GB of memory.		

needed to keep the module insulated.

4. Communication Architecture Analysis

This analysis compares four communication architectures for the C3PO payload: RS-422 wired communication, SpaceWire wired communication, 802.11n WLAN wireless communication, and the addition of an external antenna. Communication is defined here as the methods of communication between the GLL and the C3PO payload.

The following assumptions establish the basis for comparison: The work envelope is on the order of 10 to 50 m around the Griffin lander and ISRU interfaces and the propagation of wireless signals may be attenuated by the metallic structural components of C3PO's chassis [1, 18, 43].

A rough estimate for mass, power, and cost estimates for the SpaceWire, RS 422 Protocol, Wireless Communication, and Wireless Communication with Antenna are shown in Table 11. Mass is a key constraint for C3PO's mission. Power must also be taken into consideration as a system generating too much power may generate excess heat which is hard to remove.

Table 11 Mass, Power, and Cost Comparison of CCDH Communication Options. SpaceWire, RS-422, Wireless communication, and the addition of an antenna are compared. [44–46]

Option	Mass (kg)	Power (W)	Cost ($)
SpaceWire Module	0.0087	6.65	89500
RS-422 Module	0.0175	1.1	15000
Wireless Communication	0.0095	8	40000

Based on the communication range required for the mission as well as mass and cost estimates in Table 11, wireless communication was identified as the most effective primary communication method for C3PO's mission. Wireless communication offers the lowest mass solution. A concern was raised regarding Wi-Fi propagation from a payload constructed primarily of metal, as metallic enclosures can attenuate 2.4–5 GHz signals. To mitigate this, the payload can incorporate a small RF-transparent window near the Wi-Fi module to ensure reliable signal transmission. A wired option is recommended as a backup option to ensure the mission can continue if the Wi-Fi module fails. Table 11 illustrates that RS-422 modules are far more affordable and require less power than their Spacewire counterparts. Therefore, RS-422 was identified as the preferred wired interface.

5. CCDH Subsystem Design

Through the above analysis, a final CCDH subsystem was determined. The communication system will use wireless communication, connecting with the GLL through a UDP protocol to ensure accurate data transfer. The C3PO rover will also be equipped with a RS-422 module for backup wired communication in case of wireless communication failure.

The wireless communication module that was chosen for the CCDH subsystem is the BRESSNER Digi ConnectCore 91/93 series wireless embedded system-on module. The ConnectCore 91/93 series was designed based on the Digi ConnectCore i.MX53 module that was flown on NASA's Robonaut mission in 2011. The ConnectCore 91/93 was designed as a successor to the space-rated i.MX53 module. Prior to use in the C3PO mission, the 91/93 series system must be space-rated.

The Digi ConnectCore 91/93 series includes 8 GB of on-chip flash memory. Employing the Digi ConnectCore 91/93 series chip for the C3PO mission would not only address CCDH subsystem requirement of 1.5 GB transmit data, but also provide flexibility in terms of excess computational power and memory to address any data handling issues that may arise during the mission.

If space rating the chosen Wi-Fi module is not feasible, C3PO recommends employing a lockstep processing technique. With this technique, SABER would include 4 separate Digi ConnectCore Wi-Fi modules with only 2 modules active at one time. Each active module includes 2 cores available for parallel computing. Each compute task would be executed across all 4 cores simultaneously with majority voting logic to compare the outputs of each core. In the case of a single event upset (SEU), for instance a radiation particle flipping a bit, the output of 1 core will be different from the 3 remaining cores. At this point, the system will select the output of the 3 remaining cores, using majority voting logic. The processing architecture will no longer be usable when a decision with majority voting logic cannot be reached. This result would indicate an excess of tolorable radiation within the system. In this instance, the system shall power off the 2 active modules and power on the 2 idle modules to resume processing.

G. Power Generation and Storage, Thermal Control, and Environmental Protection

1. Power Requirements

Table 12 SABER Power Requirements for Mission Lifetime

Subsystem	Action	Power (W)	Energy (Wh)
PC	Material Delivery	4	4
PC	Tile Placement	4	10
SM	SABER Driving	35	72
GNC	Navigation Sensors	38	78
CCDH	FC & Comms	4	-

Table 13 GLL Power Requirements for Mission Lifetime

Subsystem	Action	Power (W)	Energy (Wh)
MI	Power Ramp	425	16,000
MI	Power Sinter	15	4,000
CCDH	RS-422 Module	1	-

Table 12 outlines the power requirements for each subsystem on SABER. The amount of power required to be generated by SABER was determined by computing the maximum power required at any given time. The most power is consumed when driving due to the drive motors and navigation sensors. For the total mission, SABER requires a peak power of 85 W and consumes an estimated energy of 164 Wh.

Table 13 outlines the power requirements for the operation of KYBER during the sintering process. The sintering process is separated into four phases. The first phase is an initial ramp-up to 1200°C that only occurs at the start of the mission. The next phase is a ten-hour sinter at 1200°C in which power is supplied on to replace lost heat. The third phase is an uncontrolled ramp-down to 750°C before ejecting the tile in which no power is consumed. The last phase is

a ramp-up back to 1200°C after the mold has been filled with more regolith. To manufacture all 25 tiles, a total energy of 20 kWh is required over 13.4 days.

Two separate power generation systems are utilized for this mission. Systems mounted to GLL such as KYBER use the power interface on the lander. The Astrobotic user guide offers three different power modes and specifies power in terms of payload mass. With a payload mass of 200 kg, wired systems have 200 W available under nominal power output. A peak power output of 500 W is available as scheduled by Astrobotic [18].

Systems not mounted to GLL such as SABER require a separate power distribution system. Power to SABER is supplied via a solar array and battery pack. The solar array was designed using SHARP IMM3J space-rated solar cells configured in 12s40p, resulting in a peak power output of 278 W [47]. Additionally, a 248.6 Wh space-rated LiPo battery pack was included to provide additional power during low-light conditions [48].

H. Thermal Control

The thermal control system for the PTE subsystem is designed to ensure survivable and operational temperatures for SABER and KYBER throughout launch, lunar transit, surface operations, and the full lunar day/night cycle. The primary thermal design challenge is maintaining the battery and temperature-sensitive electronics within allowable limits despite the extreme thermal environment at the lunar south pole, where external conditions may range from approximately -198°C during lunar night to 60°C during peak lunar day [49]. The thermal control architecture must therefore minimize heat loss during long cold conditions and reject excess internal heat during sunlit operations.

The thermal control system centers on a Warm Electronics Box (WEB), shown as a CAD rendering in 11, which houses the SABER battery, IMU, onboard computing and communications hardware, heater elements, and thermal interfaces to the radiator within an insulated enclosure. The WEB is intended to isolate critical internal components from the external environment and reduce required active heating power. The current WEB concept uses a layered wall architecture consisting of carbon-fiber-reinforced polymer (CFRP), aluminum honeycomb, aerogel insulation, and multi-layer insulation (MLI). The present concept has outer dimensions of approximately $337 \times 299 \times 239$ mm, interior dimensions of approximately $240 \times 202 \times 142$ mm, and an estimated structural mass of approximately 8.5 kg.

The passive thermal control strategy relies on three primary features: insulation, thermal isolation, and radiative heat rejection. First, MLI and aerogel reduce conductive and radiative losses between the WEB interior and the lunar environment. Second, the battery and internal electronics are packaged within the WEB to reduce exposure to external temperature swings. Third, a radiator provides controlled heat rejection during lunar day and other high-heat operating cases. Current analysis indicates that the radiator is sized to reject on the order of hundreds of watts under hot internal conditions, with preliminary estimates showing a peak rejection capability near 650 W for an internal WEB temperature near 60°C. Additional passive features under consideration include radiator placement optimization, surface optical property selection, and possible sun-shielding to reduce absorbed solar flux.

Active thermal control is provided primarily by Kapton film resistance heaters placed within the WEB and, where required, around sensitive external hardware. Preliminary transient thermal analysis suggests that only modest survival heating may be required during lunar night for the insulated WEB, on the order of 1 to 3 W continuously in the current configuration, although this value remains sensitive to final insulation performance, internal heat generation, and duty-cycle assumptions. This is well within the 10 W of continuous power that the GLL can supply SABER during lunar night. For KYBER, which includes a high-temperature heating unit, local thermal isolation and containment will be required to prevent unacceptable heat leakage into neighboring components or structural members. Thermistors and closed-loop heater control will be used to maintain acceptable component temperatures and reduce unnecessary power draw.

Thermal control performance has been assessed using preliminary transient simulations over a full lunar day/night cycle. These analyses track temperatures of the hot internal node, WEB shell, and radiator to evaluate whether the battery and other critical components remain within operational and survivable temperature limits. Early results indicate that the WEB architecture can keep internal temperatures below the survivability ceiling while also preventing excessive cold soak during lunar night. However, final heater sizing, radiator sizing, and detailed interface conductance values remain to be refined as the system layout matures. Future work will focus on validating the thermal model, refining internal heat generation assumptions, incorporating realistic boundary conditions, and converging on a flight-like thermal design through trade studies and higher-fidelity CAD-integrated simulation.

Table 14 Thermal control design summary for the PTE subsystem.

Parameter	Value
External temperature range	−198°C to 60°C
WEB outer dimensions	337 × 299 × 239 mm
WEB inner dimensions	240 × 202 × 142 mm
WEB mass	8.5 kg
Survival heating estimate	1 to 3 W
Peak radiator rejection estimate	∼ 650 W

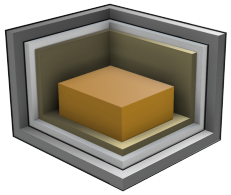

Fig. 11 Warm Electronics Box (WEB) architecture and layer stackup.

III. Conclusion

Project C3PO demonstrates a viable approach to constructing lunar surface infrastructure through in-situ resource utilization (ISRU), addressing the critical challenge of minimizing reliance on Earth-supplied materials [1]. By integrating SABER and KYBER, the architecture successfully enables excavation, processing, sintering, placement, and validation of the created pad. The resulting interlocking tile system provides a structurally robust and thermally resilient solution for mitigating dust plume effects during landing and ascent, which are known to pose significant risks to nearby equipment and infrastructure [3–6].

The system meets key mission requirements, including mass, volume, and power limitations, while maintaining operational capability in the harsh lunar environment characterized by extreme temperatures, abrasive regolith, and extended lunar night cycles [2]. The selection of oven-based sintering offers an effective balance between energy efficiency, system simplicity, and reliability, while avoiding additional mass [16, 17]. Thermal analyses indicate that the sintered tiles can withstand representative plume-induced loading conditions for the duration of the test, supporting the feasibility of the proposed technology demonstration.

The phased CONOPS ensures a logical progression from deployment to fabrication and validation. The integration of LiDAR-based mapping, vision systems, and thermal imaging provides a framework for verifying placement accuracy and material performance, ensuring compliance with mission requirements and enabling meaningful post-test analysis.

However, several limitations remain that warrant further investigation. Long-term material durability under repeated thermal cycling and cumulative plume exposure have not been fully characterized. Additionally, scaling the system to support full-size lunar parking pads will require improvements in production throughput, energy management, and system coordination. Future work should explore enhanced sintering techniques and optimized thermal control strategies to support larger-scale infrastructure development.

In conclusion, C3PO establishes a practical and scalable path toward sustainable future lunar construction by manipulating ISRU and autonomous robotic systems. As lunar exploration transitions toward permanent habitation and increased mission possibilities, such technologies will be essential for enabling safe, repeatable surface operations while reducing the logistical burden of transporting construction materials from Earth [1, 2].

Acknowledgments

The authors would like to acknowledge Dr. Shinpaugh and Tim McEvoy for providing support and guidance throughout the design process. A special thanks to Dr. Philen and Dr. Staley for offering their facilities and expertise towards sintering and testing the LSP-2 tiles. Thank you to the Kevin T. Crofton Department of Aerospace and Ocean Engineering.

References

[1] Sanders, G. B., Kleinhenz, J. E., and Hilburger, M. W., "Using ISRU and Surface Construction to Define Long-Term Lunar Infrastructure Needs," *AIAA Aviation Forum and ASCEND 2024*, American Institute of Aeronautics and Astronautics, 2024. https://doi.org/10.2514/6.2024-4840, URL http://dx.doi.org/10.2514/6.2024-4840.

[2] McKay, D. S., Heiken, G., Basu, A., Blanford, G., Simon, S., Reedy, R., French, B. M., and Papike, J., "The Lunar Regolith," *Lunar Sourcebook, A User's Guide to the Moon*, edited by G. H. Heiken, D. T. Vaniman, and B. M. French, 1991, pp. 285–356.

[3] N. J. Gelino et al., "Off Earth Landing and Launch Pad Construction—A critical technology for establishing a Long-Term presence on Extraterrestrial surfaces," , 2021. URL https://ascelibrary.org/doi/10.1061/9780784483374.079.

[4] "Lunar Landing Pads | T2 Portal," , ???? URL https://technology.nasa.gov/patent/KSC-TOPS-89.

[5] E. Mount et al., "Lunar landing and launching pad design considerations using ISRU materials," , 2025. URL https://ascelibrary.org/doi/10.1061/9780784483374.079.

[6] R. M. Kelso et al., "Planetary Basalt Field Project: Construction of a Lunar Launch/Landing Pad, PISCES and NASA Kennedy Space Center Project update," , 2021. URL https://ascelibrary.org/doi/10.1061/9780784479971.061.

[7] Jehn, Ian, "Site Preparation and Landing Pad Performance Requirements for A Lunar Human Lander System," , 2024. URL https://doi.org/10.1016/j.actaastro.2025.02.046.

[8] "A110 a M20 bipropellant, radiatively-cooled thruster for spacecraft attitude control," , ???? URL https://agilespaceindustries.com/a110.

[9] Noble, S., "05 The Lunar Regolith_noble Compressed," , ???? URL https://www.nasa.gov/wp-content/uploads/2019/04/05_1_snoble_thelunarregolith.pdf.

[10] Verbruggen, B., Zhang, X., Cowley, A., and Hadler, K., "An Automatic Dry Sieving Mechanism for a Lunar Brick Payload," *Applied Sciences*, Vol. 15, No. 4, 2025, p. 2227. https://doi.org/10.3390/app15042227, URL https://www.mdpi.com/2076-3417/15/4/2227.

[11] Katarzyna, L., Remigiusz, M., and Piotr, W., "Mathematical and empirical description of screen blocking," *Granular Matter*, Vol. 18, No. 1, 2016, p. 13. https://doi.org/10.1007/s10035-016-0622-4, URL http://link.springer.com/10.1007/s10035-016-0622-4.

[12] Cannon, K. M., Dreyer, C. B., Sowers, G. F., Schmit, J., Nguyen, T., Sanny, K., and Schertz, J., "Working with lunar surface materials: Review and analysis of dust mitigation and regolith conveyance technologies," *Acta Astronautica*, Vol. 196, 2022, pp. 259–274. https://doi.org/10.1016/j.actaastro.2022.04.037, URL https://linkinghub.elsevier.com/retrieve/pii/S0094576522001965.

[13] "How to make roads on the Moon," , ???? URL https://www.esa.int/Enabling_Support/Space_Engineering_Technology/How_to_make_roads_on_the_Moon.

[14] lassoff, s., "Tessellations: The Hidden Geometry Behind Nature's Most Efficient Structures," , Jun. 2025. URL https://stevenlassoff.substack.com/p/tessellations-the-hidden-geometry.

[15] Firefly Aerospace, "Moon Landing - Blue Ghost Makes History," , Mar. 2025. URL https://www.youtube.com/watch?v=NpHhEybJdxg.

[16] Han, W., Ding, L., Cai, L., Zhu, J., Luo, H., and Tang, T., "Sintering of HUST-1 lunar regolith simulant," *Construction and Building Materials*, Vol. 324, 2022, p. 126655. https://doi.org/10.1016/j.conbuildmat.2022.126655, URL https://doi.org/10.1016/j.conbuildmat.2022.126655.

[17] Zheng, X., Zhao, C., Sun, X., and Dong, W., "Lunar Regolith Geopolymer Concrete for In-Situ Construction of Lunar Bases: A Review," *Polymers*, Vol. 16, No. 11, 2024, p. 1582. https://doi.org/10.3390/polym16111582, URL https://doi.org/10.3390/polym16111582.

[18] Astrobotic Technology, Inc., "Lunar Landers Payload User's Guide," https://www.astrobotic.com/wp-content/uploads/2022/01/PUGLanders_011222.pdf, January 2022. Accessed: 5 Apr. 2026.

[19] Thangavelautham, J., Law, K., Fu, T., Abu El Samid, N., Smith, A. D. S., and D'Eleuterio, G. M. T., "Autonomous Multirobot Excavation for Lunar Applications," https://arxiv.org/pdf/1701.01657, January 2017. Accessed: 5 Apr. 2026.

[20] maxon, *EC 90 flat ∅90 mm, brushless, 260 W*, maxon, 2025. Catalog page, February edition.

[21] ASC 3D, "GSFL-16 LiDAR Sensor," , 2023. URL https://asc3d.com/gsfl_16k/.

[22] 3D Plus, "CASPEX 4M Space Camera with IRIS Lens," , 2023. URL https://www.3d-plus.com/products/iris-4-megapixels-space-camera/.

[23] Asnani, V., Delap, D., and Creager, C., "The development of wheels for the Lunar Roving Vehicle," *Journal of Terramechanics*, Vol. 46, No. 3, 2009, pp. 89–103. https://doi.org/10.1016/j.jterra.2009.02.005, URL https://linkinghub.elsevier.com/retrieve/pii/S0022489809000263.

[24] Rosenburg, M. A., Aharonson, O., Head, J. W., Kreslavsky, M. A., Mazarico, E., Neumann, G. A., Smith, D. E., Torrence, M. H., and Zuber, M. T., "Global surface slopes and roughness of the Moon from the Lunar Orbiter Laser Altimeter," *Journal of Geophysical Research: Planets*, Vol. 116, No. E2, 2011. https://doi.org/https://doi.org/10.1029/2010JE003716, URL https://agupubs.onlinelibrary.wiley.com/doi/abs/10.1029/2010JE003716.

[25] Rüsch, O., and Aussel, B., "The Evolution of Rock Size-Frequency Distribution on the Moon: Effects of Rock Strength and Fragmentation Products on Centimeter-Scale Abundances," *Journal of Geophysical Research: Planets*, Vol. 129, No. 10, 2024, p. e2024JE008626. https://doi.org/https://doi.org/10.1029/2024JE008626, URL https://agupubs.onlinelibrary.wiley.com/doi/abs/10.1029/2024JE008626, e2024JE008626 2024JE008626.

[26] Gläser, P., Sanin, A., Williams, J., Mitrofanov, I., and Oberst, J., "Temperatures Near the Lunar Poles and Their Correlation With Hydrogen Predicted by LEND," *Journal of Geophysical Research: Planets*, Vol. 126, No. 9, 2021, p. e2020JE006598. https://doi.org/10.1029/2020JE006598, URL https://agupubs.onlinelibrary.wiley.com/doi/10.1029/2020JE006598.

[27] Li, Y., and Wu, B., "Analysis of Rock Abundance on Lunar Surface From Orbital and Descent Images Using Automatic Rock Detection," *Journal of Geophysical Research: Planets*, Vol. 123, No. 5, 2018, pp. 1061–1088. https://doi.org/10.1029/2017JE005496, URL https://agupubs.onlinelibrary.wiley.com/doi/10.1029/2017JE005496.

[28] Ullrich, F., Goktog˘an, A. H., and Sukkarieh, S., "Design Optimization of a Mars Rover's Rocker-Bogie Mechanism using Genetic Algorithms," ????

[29] Harmonic Drive LLC, *SHF-20-160-2UH Harmonic Drive Gear*, Harmonic Drive LLC, Beverly, MA, ???? Technical datasheet.

[30] Wang, S., Zou, M., Dang, Z., Chen, B., Zhou, T., and Su, B., "Modelling of flexible metal wheels for planetary rover on deformable terrain," *Thin-Walled Structures*, Vol. 141, 2019, pp. 97–110.

[31] Thrun, S., Burgard, W., and Fox, D., *Probabilistic Robotics*, MIT Press, 2005.

[32] Cadena, C., Carlone, L., Carrillo, H., Latif, Y., Scaramuzza, D., Neira, J., Reid, I., and Leonard, J. J., "Past, Present, and Future of Simultaneous Localization and Mapping: Toward the Robust-Perception Age," *IEEE Transactions on Robotics*, Vol. 32, No. 6, 2016, pp. 1309–1332. https://doi.org/10.1109/TRO.2016.2624754.

[33] "Localization and Mapping for Mars Rover Navigation," *Science*, 2010. https://doi.org/10.1126/science.1187726.

[34] Automotive Electronics Council, "AEC-Q100: Failure Mechanism Based Stress Test Qualification for Integrated Circuits," , 2014. URL https://www.aecouncil.com/Documents/AEC-Q100_Rev_G.pdf.

[35] Safran Navigation & Timing, "STIM377H Inertial Measurement Unit," , 2023. URL https://safran-navigation-timing.com/product/stim377h-inertial-measurement-unit-imu/.

[36] INO, "HDISCC Thermal Camera," , 2023. URL https://solar-mems.com/space-equipment/nanossoc-d60/.

[37] Solar MEMS, "nanoSSOC-D60 Sun Sensor," , 2023. URL https://solar-mems.com/space-equipment/nanossoc-d60/.

[38] Netzer Precision, "VLS-25-II Encoder," , 2023. URL https://netzerprecision.com/products/vls-25/.

[39] *RS9113 Module Family Datasheet*, Redpine Signals, Inc., San Jose, CA, 3rd ed., Jan. 2018. URL https://www.mouser.com/datasheet/2/368/RS9113_Module_Family_Datasheet-3079635.pdf, accessed: 2025-12-06.

[40] *WL18x7MOD WiLink™ 8 Dual-Band Industrial Module – Wi-Fi®, Bluetooth®, and Bluetooth Low Energy (LE)*, Texas Instruments, Dallas, TX, rev. l ed., May 2025. URL https://www.ti.com/lit/ds/symlink/wl1837mod.pdf, accessed: 2025-12-06.

[41] OptCore, "Difference Between RS-232, RS-422, and RS-485," https://www.optcore.net/difference-between-rs-232-rs-422-and-rs-485/, 2023. Accessed: 2025-11-19.

[42] STAR-Dundee Ltd., "An Overview of the SpaceWire Standard," https://www.star-dundee.com/spacewire/getting-started/an-overview-of-the-spacewire-standard/, 2025. Accessed: 2025-11-19.

[43] Astrobotic Technology Inc., "Griffin Lunar Lander Technical Overview," , 2021. URL https://www.astrobotic.com/lunar-delivery/landers/griffin-lander/.

[44] SIEMENS, "CM 1241 RS422/485 specifications," https://docs.tia.siemens.cloud/r/simatic$_s$7$_1$200$_m$anual$_c$ollection$_i$tit$_2$0/$technical-specifications/bb-1297-battery-board, Nov2024.

[45] Elham Serria, S. A. H. M. A. C. R. A.-A. F. L. W. M., Rida Gadhafi, "A Review of Lunar Communications and Antennas: Assessing Performance in the Context of Propagation and Radiation," https://pmc.ncbi.nlm.nih.gov/articles/PMC10748255/, Dec 2023.

[46] SpaceWire, "Cables," https://www.star-dundee.com/spacewire/spacewire-users-guide/spacewire-links/physical-level/cables/, Nov 2025.

[47] Sharp, "Sharp IMM3J Datasheet," , ???? URL https://global.sharp/solar/en/space-qualified/pdf/datasheet_IMM3J.pdf.

[48] ABSL, "Product Data Sheet Li-ion Rechargeable Battery ABSL 8s3p 28V 8.4Ah," , ???? URL https://www.enersys.com/49a4e6/globalassets/documents/product-documentation/absl/amer/amer-en-fly-absl-8s3pmm_0424.pdf.

[49] Lunarpedia, "Lunar Temperature," https://lunarpedia.org/w/Lunar_Temperature, 2011. Last modified November 10, 2011; accessed April 9, 2026.